第 38 卷第 2 期 分 子 催 化（中 英 文） Vol.38,No.2
2024 年 4 月 JOURNAL OF MOLECULAR CATALYSIS(CHINA) Apr. 2024

Article ID：1001-3555(2024)02-0099-05 *Articles*

Synthesis and Properties of Two-dimensional Composite Photocatalyst

LI Jing*, LI Quan-sheng

(China National Building Materials (Hefei) New Energy Resources Co., Ltd, Hefei 230000, China)

Abstract: A novel two-dimensional photocatalyst BiOCl/MOF-5 was successfully synthesized *via* a facile ultrasonic assisted solvothermal method. The X-ray diffraction, Scanning Electron Microscope, Transmission Electron Microscope, Brunauer-Emmett-Teller, UV-Visible diffuse reflectance spectrum and photoluminescence were employed to characterize and investigate its unique structure and property. In this photocatalytic system, MOF-5 was chosen as a substrate and combined with BiOCl catalyst to achieve a fire-new two-dimensional composite. The results showed that the synthesized BiOCl/MOF-5 composite photocatalyst all present a good two-dimensional morphology, and the specific surface area (110.16 $m^2 \cdot g^{-1}$) is significantly higher than that of single BiOCl (3.15 $m^2 \cdot g^{-1}$). Comparing with the pure BiOCl, the composite photocatalyst exhibits outstanding photocatalytic activity in the degradation of organic pollutants. Due to the unique structure and characteristics of MOF-5, the problem of composite catalyst aggregation and the small specific surface area is well solved. In addition, relative large specific surface area and appropriate energy band gap are beneficial for the photocatalytic reactions by providing more active sites and efficient transport paths for reactants. The photocatalytic properties of catalysts are closely related to their specific surface area and pore volume. Hence, the photocatalytic activity is obviously improved.

Key words: 2D photocatalyst; ultrasonic assisted solvothermal; BiOCl/MOF-5; photocatalytic performance

CLC number: O643.36 **Document code:** A **DOI:** 10.16084/j.issn1001-3555.2024.02.001

In the process of industrialization development, the environmental pollution has seriously affected people's daily life, and at the same time, the demand for energy consumption is also increasing. As a green, efficient and clean technology, photocatalytic technology has an important application prospect in the field of energy and environment with its advantages of direct utilization of solar energy [1−4]. As one of the most significant components of photocatalytic technology, the photocatalyst developments have been the focus of public attention and research.

BiOCl, a novel 2D layered ternary oxide semiconductor, has been found to be potential photocatalytic ability. However, the photocatalytic activity of pure BiOCl is limited due to its low efficiency of light absorption, low adsorption capacity, and high recombination rate of photoinduced electron-hole pairs[5−7]. To overcome these problems, an effective strategy is incorporating them with other functional species to form BiOX-based composites[8−9]. Hence, there are two methods to improve the potential of BiOCl for photocatalytic application, one is the effective separation of the photogenerated electrons and holes[10−12]. For instance, Mokhtari *et al*. successfully prepared W-doped BiOCl nanosheets, and it shows that excellent photocatalytic performance for the degradation of RhB compared with pure BiOCl in both UV and visible light. This is attributed to gap and expanded light absorption region[13]. Zhang *et al*. have been synthesized Fe-doped BiOCl to degrade levoflo-xacin. The results show that the pholocatalyst has excellent photocatalytic degradation performance and excellent reuse performance. The photocatalytic degradation efficiency can reach 95% within 60 min[14]. The other is the increase of accessible surface area for more contact of target molecules[15−17]. Metal-organic frameworks (MOFs), which are built by the coordination of metal ions and organic linkers, showing a variety of strengths such as various species, designable and adjustable structure, low crystal density and high specific surface area compared with porous molecular sieve and acticarbon [18−22]. At present, it has become a research frontier and hot point in the material field. These factors render it an ideal candidate for the development of BiOX nanosheet-based heterogeneous composite to improve the photocatalytic performance of the catalyst [23−24].

In this study, a novel two-dimensional photocatalyst BiOCl/MOF-5 was prepared by ultrasonic assisted solvo-thermal method. Herein, MOF-5 was chosen as a substrate, combined with the novel BiOCl catalyst to achieve a fire-new composite. Comparing with some recent research materials [6], the prepared composite exhibits an outstanding photocatalytic activity in degradation of organic contaminant. Benefiting from the unique structure and characteristics of MOF-5, the problems of composite catalyst aggregation and the small specific surface area are improved reduced. Hence, compared with the pure BiOCl, the photocatalytic activity of BiOCl/MOF-5 is obvious-ly enhanced.

1 Experimental

1.1 BiOCl synthesis

BiOCl was synthesized following the procedure described. Firstly, 10 mmol of $Bi(NO_3)_3 \cdot 5H_2O$ and 10 mmol of KCl were added to 20 mL solvent of water, respectively. Then, KCl solution was slowly dripped into $Bi(NO_3)_3 \cdot 5H_2O$ solution under ultrasonic condition and stirred for 1 h subsequently. Following

Received date: 2023-12-20; **Revised date:** 2024-02-15.

Biography: LI Jing(1992–), female, engineer, mainly engaged in research of energy functional materials and photocatalysis.

* Corresponding authors. E-mail: 2538848026@qq.com.

one hour of stirring, the final solution was heated at 160 ℃ for 12 h in a Teflon-lined stain-less autoclave. Washed the white powder with water and ethanol for three times and dried at 80 ℃. Finally, BiOCl nanoparticles were prepared.

1.2 BiOCl/MOF-5 synthesis

MOF-5 was synthesized following the procedures described. Firstly, $Zn(CH_3COO)_2{\cdot}2H_2O$ and H_2BDC were dissolved in 30 mL of DMF at a molar ratio of 3∶1. Following several minutes of stirring, the obtained mixture was sealed in a closed vessel by ultrasonic instrument. After ultrasonic 80 min, the mixed solution was heated at 120 ℃ for 24 h in a Teflon-lined stainless autoclave. Centrifugation was done for the collection of the product proceeding to repeated washing with DMF. Later on, the final product was dried out at 80 ℃ in vacuum conditions. Finally, two-dimensional MOF-5 crystal was obtained.

Based on the as-prepared materials, a certain amount of MOF-5 and BiOCl were respectively dispersed into 20 mL DMF by ultrasonic instrument. Afterwards, MOF-5 suspension was slowly introduced into BiOCl suspension. Following several minutes of stirring, the mixture was transferred into a Teflon-lined stainless steel autoclave. After heated at 120 ℃ for 24 h, the product was cooled down to room temperature in air. Later on, the samples were collected and washed several times and then dried at 80 ℃.

2 Results and Discussion

2.1 XRD Analysis

The crystallographic structures of the as-synthesized MOF-5, BiOCl and BiOCl/MOF-5 composites were determined by XRD analysis, as shown in Fig. 1. It shows that the pristine BiOCl sample was well crystallized and the diffraction peaks can well be indexed to the tetragonal BiOCl (JCPDS Card No. 06-0249)[25]. Interestingly, the intensity of the diffraction peaks in the BiOCl/MOF-5 system differs from that of BiOCl. Thus, it is expected that MOF-5 may influence the exposed percentage of crystal planes of BiOCl. Otherwise, no other diffraction peaks appear in the composite structure BiOCl/MOF-5, indicating no other impurities in the XRD test range.

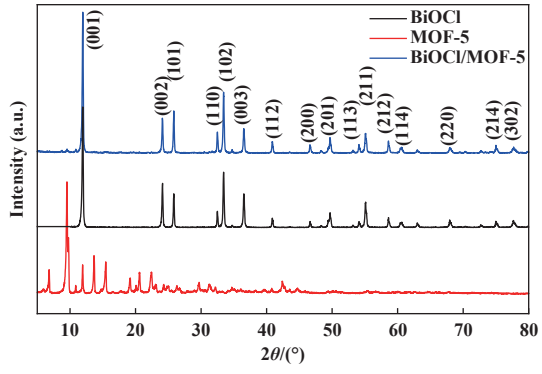

Fig.1 XRD patterns of different samples

2.2 SEM and TEM analysis

The morphologies of the as-synthesized BiOCl and BiOCl/MOF-5 were characterized by SEM analysis. The sample of BiOCl (Fig. 2(a)) exhibits the representative sheet-like structure. Fig. 2(c) displays the SEM images of BiOCl/MOF-5 materials. Compared with BiOCl, a similar sheet-like morphology can be observed. In Fig. 2(b), the pristine MOF-5 that developed by the ultrasonic-assisted solvothermal method consisted of plenty of two-dimensional sheet-like structures, rather than the common cubic structure. In the wake of the further introduction of MOF-5, Fig. 2(c)shows that, compared with the pure BiOCl, the surface roughness and thickness of BiOCl/MOF-5 was increased, but still shows a distinct two-dimensional morphology. These results indicate that the major morphology of the BiOCl sample was not significantly altered by the introduction of MOF-5. The microstructures of the BiOCl/MOF-5 composites were further investigated by TEM. The TEM images (Fig. 2(d)) confirmed the 2D structure of the BiOCl/MOF-5 composites clearly.

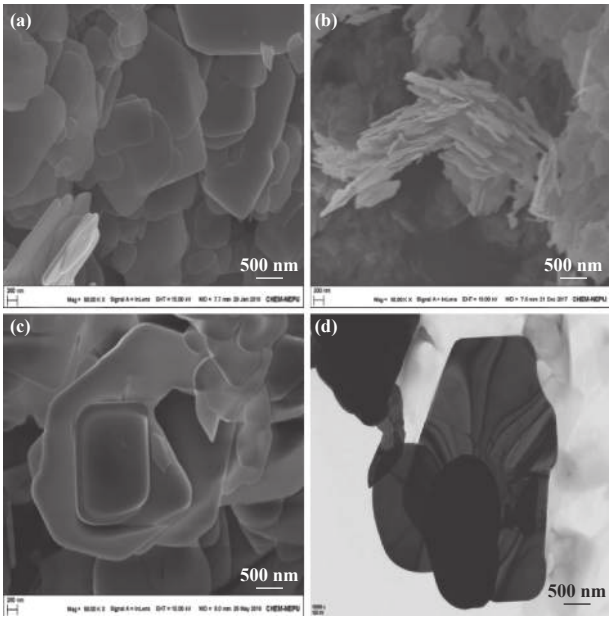

Fig.2 SEM((a) BiOCl; (b) MOF-5; (c) BiOCl/MOF-5) and TEM ((d) BiOCl/MOF-5) images of different samples

2.3 BET analysis

Fig. 3 illustrates the adsorption-desorption isotherms and pore diameter distribution curves of BiOCl and BiOCl/MOF-5. Table 1 summarizes the BET surface area and pore volume of as-synthesized samples. The specific surface area is increased from 3.15 to 110.16 $m^2{\cdot}g^{-1}$ after recombination. We can find that after modification of BiOCl by MOF-5, the surface area and pore volume of BiOCl/MOF-5 were higher than those of pure BiOCl, which is beneficial for the photocatalytic reactions by providing more active sites and efficient transport paths for reactants. The photocatalytic properties of catalysts are closely related to their specific surface area and pore volume. Thus, the large specific surface area and pore volume of BiOCl/MOF-5 might play a role in enhancing the photocatalytic activity.

2.4 UV-Vis DRS and PL spectra analysis

Fig. 4 shows in the UV-Vis DRS and PL spectra of different samples. As shown in Fig. 4(a), the optical absorption properties and the band gap energy of as-prepared samples were investigated by using UV-Vis diffuse reflectance spectroscopy. It is well known that the bandgap of semiconductors can be calculated by the following formula $\alpha h\nu = A(h\nu - E_g)^{n/2}$, where α, h, ν, E_g and A are absorption coefficients, Plank constant, light frequency, bandgap and constant, respectively[13], n

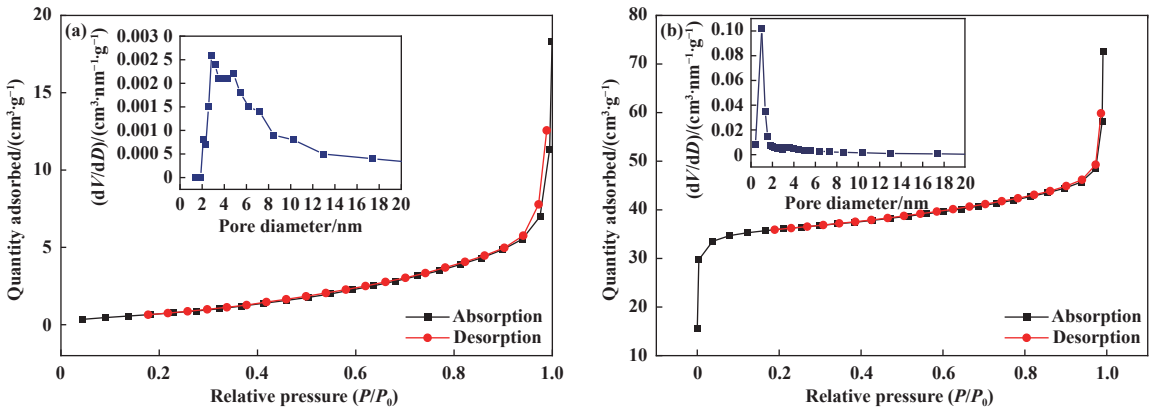

Fig.3 N_2 adsorption-desorption isotherms and pore size distribution curves of different samples

Table 1 Specific surface area (A_{BET}) and pore volume (V_{BET}) of different samples

Catalyst samples	A_{BET}/(m^2·g^{-1})	V_{BET}/(cm^3·g^{-1})
BiOCl	3.15	0.028
BiOCl/MOF-5	110.16	0.110

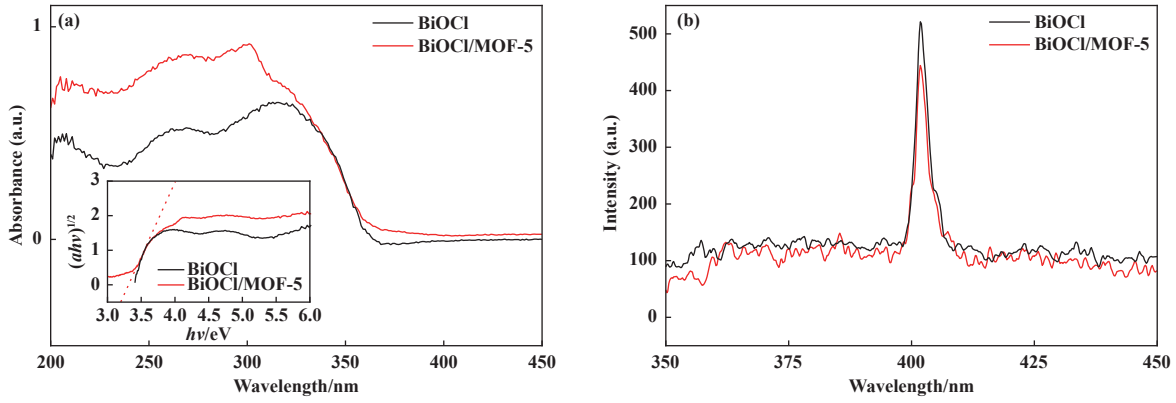

Fig.4 (a) UV-Vis DRS and (b) PL spectra analysis for the optical properties of different samples

surface area of the composite structure in the specific surface area of the lifting material, and has no obvious damage to the electronic structure of a single structure.

Fig. 4(b) displays PL spectra of BiOCl and BiOCl/MOF-5. We can see that the BiOCl/MOF-5 exhibit peaks at similar positions, but the intensity of the composite peaks is lower than that seen for bare BiOCl. Lower PL intensities point to slower recombination of electron - hole pairs, suggesting more photo - excited holes and electrons can participate in redox reactions, thereby enhancing photocatalytic performance.

2.5 Photoreactivity

In order to further explain the effect of BiOCl/MOF-5 on the degradation of RhB in the reaction system, the degradation rate and TOC in the reactive solution at different reaction time were detected. As shown in Fig. 5(a), with the increase of reaction time, the degradation rate of RhB solution and the removal rate of TOC increase gradually. It can see that pure BiOCl has limited photocatalytic activity, and the RhB degradation ratio is 59.9% after simulated solar light irradiation. As for BiOCl/MOF-5 composites, they universally possessed better photocatalytic performance than the pure photocatalyst. The RhB degradation ratio increases to 83.5% when BiOCl combines with MOF-5. And after 5 h visible-light irradiation, about 95.5% of the TOC were removed by using BiOCl/MOF-5 as photocatalyst. The result indicates that BiOCl/MOF-5 photocatalyst could effectively mineralize RhB molecules into CO_2, H_2O and other inorganic products. Accordingly, the as-prepared ultrathin BiOCl/MOF-5 composites showed high degradation rate and TOC removal efficiency of RhB.This may be attributed to MOF-5 which can increase the accessible surface area and contact more RhB molecules, and the ZnO node of the framework can promote the effective separation of the photogenerated electrons and holes.

The photocatalyst stability is a very important parameter for practical applications. The as-prepared BiOCl/MOF-5 composite photocatalyst was also evaluated, as shown in Fig. 5(b). It can see that the photocatalyst exhibited excellent reusability for up to four consecutive cycles, indicating that the samples were highly stable during the photocatalytic oxidation of the organic contaminants, which ensured its application in practical fields.

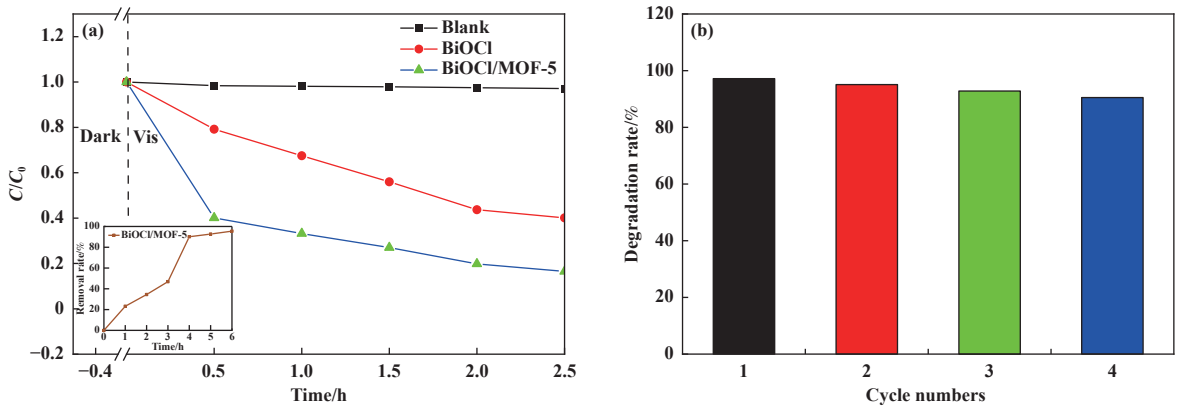

Fig.5 Photodegradation of different samples for RhB

2.6 Simulated formation process

Fig. 6 shows the simulated formation process. First place, $Bi(NO_3)_3·5H_2O$ and KCl were reacted in solution to generate a large number of BiOCl nuclei. In liquid reaction, the formation is due to the layer structure and low surface energy of the {001} facets of BiOCl. The surface atoms structure reveals that the {001} facets of BiOX contain terminal oxygen atoms, and {001} facets are expected to be more negatively charged. Therefore, when the solvent is water, H^+ binds to the O atom of the (001) crystal surface of BiOCl to reduce its surface energy, resulting in the (001) crystal surface of BiOCl becoming stable, and finally grows into a BiOCl nanosheet with a high exposure (001) crystal surface. Then, the MOF-5 suspension was slowly dropped into the BiOCl solution, and the BiOCl was slowly and uniformly dispersed on the MOF-5 surface, slowly spreading from the relatively aggregated state. Finally, with the introduction of MOF-5, a new two-dimensional nanolamellar structure was formed. To some extent, the composite with 2D structure increases its active surface area, providing more active sites and thus fully catalyze the degradation of pollutants.

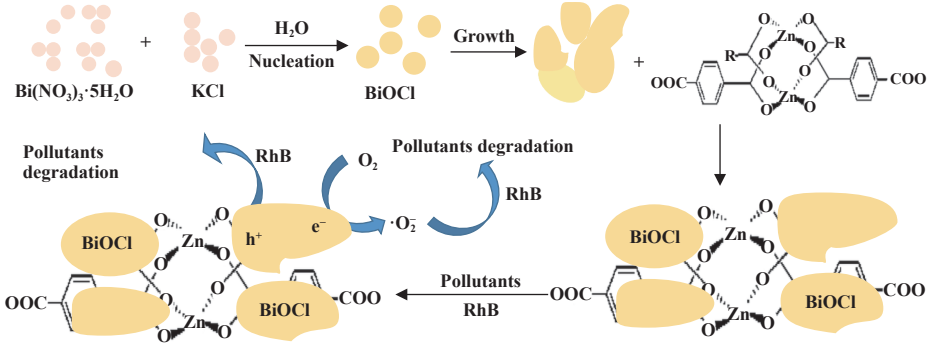

Fig.6 Simulated formation process of BiOCl/MOF-5 catalyst

2.7 Photocatalytic mechanism

On the basis of the experimental studies, the possible reaction mechanism of the photocatalytic procedure is proposed and illustrated in Fig. 7. After sunlight begins the irradiation, the photoelectrons on the surface of BiOCl can easily migrate to MOF-5 because the CB of BiOCl is lower than the LUMO of MOF-5. Similarly, the h^+ located in MOF-5 can also migrate into the VB of BiOCl. Then, the photoelectrons are trapped by oxygen, reduced to generate active species ($•O^{2-}$) and the h^+ left in BiOCl reacts with pollutants to produce H_2O and CO_2. Subsequently, h^+ and e^- migrated to the surface of BiOCl/MOF-5 photocatalyst, thus the recombination of photogenerated electron-hole pairs can be effectively inhibited and the corresponding photocatalytic properties would be greatly improved.

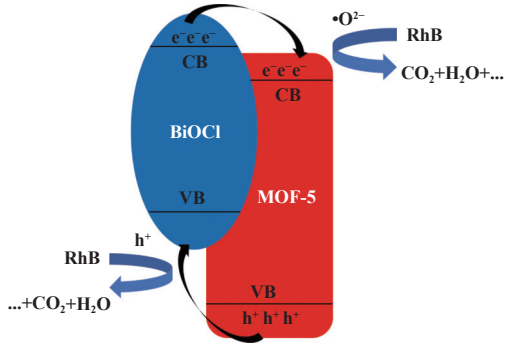

Fig.7 The possible reaction mechanism of the photocatalytic procedure

3 Conclusions

In this study, we used a novel method to synthesize two-dimensional composite photocatalyst *via* a simple hydrothermal route with the aid of ultrasonic assistance. Compared with pure BiOCl, the specific surface area of the BiOCl/MOF-5 is increased from 3.15 to 110.16 $m^2·g^{-1}$, when MOF-5 coupled with BiOCl. The results show that BiOCl/MOF-5 sample exhibited a remarkably higher photocatalytic activity for degrading RhB than BiOCl sample. This 2D structure of BiOCl/MOF-5 can provide efficient transport paths for

reactants and more active sites for the photocatalytic reaction. These results would not only provide appropriate reference for the new development of MOF-based hybrid materials, but also facilitate the reasonable design and performance enhancement of photocatalysts.

References

[1] a. Jiang X, Fuji M. *In-situ* preparation of black TiO_2/Cu_2O/Cu composites as an efficient photocatalyst for degradation pollutants and hydrogen production[J]. *Catal Lett*, 2022, **152**(11): 3272−3283.
b. Chen S T, Wang H, Cui W Q. Iron-doped bismuth sulfide Photo-Fenton degrades organic pollutants[J]. *J Mol Catal (China)*, 2024, **38**(1): 17−25.
c. Li C X, Jia M L, Guo S H, *et al*. Research progress of carbon dioxide photoreduction based on the catalyst of metal nano-clusters[J]. *J Mol Catal (China)*, 2023, **37**(6): 614−624.

[2] Song S, Xing Z, Zhao H, *et al*. Recent advances in bismuth-based photocatalysts: Environment and energy applications[J]. *Green Energy Environ*, 2023, **8**(5): 1232−1264.

[3] Wang H, Zhang Q, Qiu M, *et al*. Synthesis and application of perovskite-based photocatalysts in environmental remediation: A review[J]. *J Mol Liq*, 2021, **334**: 116029.

[4] Abdullah A, Ebrahim A S, Sadia R, *et al*. Recent advances in constructing heterojunctions of binary semiconductor photocatalysts for visible light responsive CO_2 reduction to energy efficient fuels: A review[J]. *Int J Energ Res*, 2021, **46**(5): 5523−5584.

[5] Xu S, Gao X, Xu W, *et al*. Tunable synthesis of ultrathin BiOCl 2D nanosheets for efficient photocatalytic degradation of carbamazepine upon visible-light irradiation[J]. *J Chem*, 2020, **2020**(5): 1950645.

[6] Ebrahim K, Kuo D H, Duresa L W. Synthesis and characterizations of BiOCl nanosheets with controlled particle growth for efficient organic dyes degradation[J]. *J Ind Eng Chem*, 2019, **83**: 200−207.

[7] Zhao A, Zhang L, Guo Y, *et al*. Emerging members of two-dimensional materials: Bismuth-based ternary compounds[J]. *2D Mater*, 2021, **8**(1): 012004.

[8] Wang X, Yan J, Wang H, *et al*. Enhanced degradation of carbamazepine by BiOX (Cl, Br, I) composite photocatalysts under simulated solar light irradiation[J]. *Chem Phys Lett*, 2022, **787**: 139222.

[9] Raza A, Qin Z, Li G, *et al*. Recent advances in structural tailoring of BiOX-based 2D composites for solar energy harvesting[J]. *J Envrion Chem Eng*, 2021, **9**(6): 106569.

[10] He Y, Li J, Li K, *et al*. Bi quantum dots implanted 2D C-doped BiOCl nanosheets: Enhanced visible light photocatalysis efficiency and reaction pathway[J]. *Chin J Catal*, 2020, **41**(9): 1430−1438.

[11] Xiao X, Lu M, Zhang Z. Novel Z - scheme 2D/2D $Bi_4O_5Br_2$/BiOCl heterojunction with enhanced photocatalytic activity for RhB degradation[J]. *J Chem Technol Biotechnol*, 2022, **97**(5): 1280−1292.

[12] Jiang Z, Yang Z, Shu J, *et al*. $Zn_{0.5}Cd_{0.5}S$ nanoparticle modified 2D BiOCl as solid-state Z-scheme photocatalyst for enhanced rhodamine B removal[J]. *Colloid Surf A*, 2022, **644**: 128898.

[13] Mokhtari F, Tahmasebi N. Hydrothermal synthesis of W-doped BiOCl nanoplates for photocatalytic degradation of rhodamine B under visible light[J]. *J Phys Chem Solids*, 2021, **149**: 109804.

[14] Zhong X, Zhang K, Wu D, *et al*. Enhanced photocatalytic degradation of levofloxacin by Fe-doped BiOCl nanosheets under LED light irradiation[J]. *Chem Eng J*, 2020, **383**: 123148.

[15] Li H , Long B , Ye K , *et al*. A recyclable photocatalytic tea-bag-like device model based on ultrathin Bi/C/BiOX (X = Cl, Br) nanosheets [J]. *Appl Surf Sci*, 2020, **515**: 145967.

[16] Ma H, Liu J, Zuo S. One-step fabrication of 2D/2D Z-Scheme BiOCl/*g*-C_3N_4 nanosheets heterojunction for efficient degradation of RhB and Cr(VI) ions reduction under visible-light illumination[J]. *ChemistrySelect*, 2021, **6**(37): 10097−10104.

[17] Hou J, Zhang T, Jiang T, *et al*. Fast preparation of oxygen vacancy-rich 2D/2D bismuth oxyhalides-reduced graphene oxide composite with improved visible-light photocatalytic properties by solvent-free grinding[J]. *J Clean Prod*, 2021, **328**: 129651.

[18] Thong C H, Priyanga N, Ng F L. Metal organic frameworks (MOFs) as potential anode materials for improving power generation from algal biophotovoltaic (BPV) platforms[J]. *Catal Today*, 2022, **397**: 419−427.

[19] Yang H, Jia L, Zhang Z, *et al*. Novel cerium-based MOFs photocatalyst for photocarrier collaborative performance under visible light[J]. *J Catal*, 2022, **405**: 74−83.

[20] Xiao Y, Guo X, Yang N, *et al*. Heterostructured MOFs photocatalysts for water splitting to produce hydrogen[J]. *J Energy Chem*, 2021, **58**(7): 508−522.

[21] Yun R, Hu Y, Sheng T, *et al*. Nano-Ni-MOFs: High active catalysts on the cascade hydrogenation of quinolines[J]. *Catal Lett*, 2021, **151**(8): 2445−2451 .

[22] Ma Z, Guan B, Guo J. State of the art and prospectives of heterogeneous photocatalysts based on metal-organic frameworks (MOFs): Design, modification strategies, and their applications and mechanisms in photodegradation, water splitting, and CO_2 reduction[J]. *Catal Sci Technol*, 2023, **13**(15): 4285−4347.

[23] Lou W, Wang L, Zhang Y, *et al*. Synthesis of BiOBr/Mg metal organic frameworks catalyst application for degrade organic dyes rhodamine B under the visible light[J]. *Appl Organomet Chem*, 2021, **35**(9): e6324.

[24] Qu Y, Chen Z, Duan Y, *et al*. H_2O_2 assisted photocatalysis over Fe - MOF modified BiOBr for degradation of RhB[J]. *J Chem Technol Biotechnol*, 2022, **97**(10): 2881−2888.

[25] Grilla E, Kagialari M N, Petala A, *et al*. Photocatalytic degradation of *Valsartan* by MoS_2/BiOCl heterojuctions[J]. *Catalysts*, 2021, **11**(6): 650.

二维复合光催化剂的合成及其性能研究

李　静*, 李全胜

（中建材 (合肥) 新能源有限公司, 安徽 合肥 230000）

摘要: 通过超声辅助溶剂热法制备一种新型的二维类复合光催化剂 BiOCl/MOF-5. 运用 XRD、SEM、BET、TEM、PL 等手段对催化剂的特殊结构和性能进行表征. 在该光催化剂体系中, 选取 MOF-5 为载体, 通过与光催化剂 BiOCl 复合来合成一种新型的二维复合光催化剂. 结果表明, 制备的催化剂均呈现出较为明显的二维结构形貌, 且相对于单一 BiOCl (3.15 $m^2 \cdot g^{-1}$) 来说, 该复合催化剂 (110.16 $m^2 \cdot g^{-1}$) 的比表面积得到了明显的提高. 由于催化剂的光催化性能与其比表面积和孔隙体积密切相关, 复合催化剂相对较大的比表面积和适当的能带隙, 有利于为反应物提供更多的活性位点和有效的传输路径. 得益于 MOF-5 独特的形貌和结构, 光催化剂聚集和比表面积小的问题也得到了解决. 因此, 该复合材料在降解有机污染物方面呈现出优异的光催化活性, 且与纯 BiOCl 相比, 催化剂的光催化活性得到了明显的提高.

关键词: 二维光催化剂; 超声辅助溶剂热; BiOCl/MOF-5; 光催化性能